Cite this article as:
F. Giacalone, F. Vassallo, F. Scargiali, A. Tamburini, A. Cipollina, G. Micale, The first operating Thermolytic Reverse Electrodialysis Heat Engine, *Journal of Membrane Science 595 (2020) 117522*
https://doi.org/10.1016/j.memsci.2019.117522

The first operating Thermolytic Reverse Electrodialysis Heat Engine

F. Giacalone[a], F. Vassallo[a], F. Scargiali[a], A. Tamburini[a], A. Cipollina*[a], G. Micale[a]

[a]*Dipartimento di Ingegneria, Università degli Studi di Palermo (UNIPA)- viale delle Scienze Ed.6, 90128 Palermo, Italy.*

*corresponding author: andrea.cipollina@unipa.it ù

Abstract

Thermolytic reverse electrodialysis heat engine (t-RED HE) has been recently proposed as a technology for converting low-temperature waste heat into electricity. The construction and operation of the first world lab-scale prototype unit are reported. The system consists of: (i) a reverse electrodialysis unit where, the concentration gradient between two solutions of thermolytic salts is converted into electricity and (ii) a thermally-driven regeneration unit where low-temperature heat is used to restore the initial conditions of the two feed streams. Regeneration is based on a degradation process of salts into gas ammonia and carbon dioxide, which can be removed almost entirely from the exhausted dilute solution by vapour stripping and, subsequently, reabsorbed into the exhausted concentrate solution, thus restoring the initial salinity gradient of the two streams. For the first time, the feasibility of the process was demonstrated through an experimental campaign to evaluate the system performance via long-run tests

Keywords: *Ammonium Bicarbonate solutions, salinity gradient power, osmotic power, waste heat recovery, low-grade heat.*

Introduction

The recovery and re-use of waste heat contribute to increase the efficiency of industrial plants, reducing energy costs and CO_2 emissions. Referring to the industrial sector, a huge amount of the energetic input (20-50%) is lost as waste heat contained in hot liquid and gaseous streams [1].

In the United States [2], almost 10^4 TWh of carbon, natural gas and nuclear energy were converted in $3.4 \cdot 10^3$ TWh of electricity with an average efficiency of 32 %, releasing in the environment about $5.25 \cdot 10^3$ TWh of waste heat. It has been estimated that in UK[3] about 14.4 TWh of low temperature waste heat is discharged to the environment. This amount is equal to 4% of the global energy consumption [3]. Waste heat recovery has been shown to offer economic savings of about £100 mil/yr, with the added benefit of reducing CO_2 emissions by potentially millions of tons per year. Waste heat sources are classified in three different levels according to the temperature: (i) high temperature waste heat ($T > 650\ ^\circ C$), (ii) medium temperature waste heat ($230\ ^\circ C < T < 650\ ^\circ C$) and (iii) low temperature waste heat ($T<230^\circ C$). Papapetrou et al. reported a potential of about 300 TWh/year of waste-heat from EU industrial sector in 2015, of which about 60% available at temperature below 200°C.[4]

Heat recovery technologies are classified primarily as active or passive. Passive technologies (e.g. heat exchangers and thermal energy storage) are based on re-using directly the waste-heat at the same or lower temperature level than the heat source. Conversely, active technologies are based on the upgrade of heat into a higher temperature level or on the conversion into another form of useful energy. The active technology can be classified in: (i) “waste-heat to heat”, (ii) “waste-heat to cold” and (iii) “waste-heat to power”. For this latter case, Steam Rankine Cycle, Organic Rankine Cycle [5] and Kalina Cycle [6] are examples of conventional technologies.

Recently, different innovative technologies have been proposed in the literature [7] such as Thermoelectric Generator [8,9], Stirling Engine [10], Carbon Carrier cycle [11], Thermally Regenerative Ammonia-based Battery [12] and Salinity Gradient Power Heat Engine (*SGP-HE*), all suitable for converting low-grade heat into electricity.

Salinity Gradient Power (*SGP*) or Salinity Gradient Energy (*SGE*) is a sustainable energy source, which was identified for the first time in the 1950s by Pattle [13]. This energy source is based on harvesting the Gibbs free energy released during the mixing of salt solutions at different

concentration. Pressure retarded osmosis (*PRO*) and reverse electrodialysis (*RED*) are the main *SGP* technologies proposed so far.

PRO makes use of osmotic membranes to convert the salinity gradient between two solutions into a water flux, from the dilute to the concentrate, "retarded" from the application of a hydraulic pressure in the concentrate side. Thus, the permeate water "gains" pressure energy, which is eventually converted into mechanical and electrical energy through a hydraulic turbine.

In the *RED* process, Ion Exchange Membranes (*IEM*s) are used to convert the concentration difference between two solutions into an ionic current. A *RED* unit consists of a stack in which cation and anion exchange membranes are alternatively piled. The compartments between two different membranes are alternatively fed with concentrate and dilute solutions. Membrane solution interface equilibria and selective ions transport phenomena lead to the generation of an electro-motive force accompanied by an ionic current, which make of a RED unit a perfect power generator.

SGP-HE is a coupled system consisting of (i) a *SGP* unit (i.e. the power unit) in which electricity is produced exploiting the salinity gradient of two solutions and (ii) a thermal regeneration unit, where low-grade waste heat is used to restore the initial concentration of the two solutions. One of the main advantages of using a closed-loop *SGP-HE* configuration, rather than open-loop *SGP*, is the possibility to use ad-hoc salt-water solutions in order to enhance the performance of the system. Among the different salt-solutions proposed so far, the use of thermolytic salts, such as ammonium bi-carbonate (NH_4HCO_3), has been presented as a promising opportunity [14], due to the potential use of very-low grade heat (40-100°C) to regenerate the solutions by means of thermal degradation and stripping/absorption processes. In fact, heating up the NH_4HCO_3 solutions above 40-60°C, the ions undergo a degradation process, which promotes the formation of gaseous compounds, NH_3 and CO_2, easily removable from solution [15].

The idea to convert waste-heat into electricity through closed-loop *SGP* technologies was theoretically proposed for the first time by S. Loeb in 1974 for *PRO* [16] and in 1979 for *RED* [17]. However, only in recent years, thanks to the development of new membranes and process schemes, the idea of Loeb led to the first experimental efforts to characterise the behaviour of the *RED-HE* systems. Luo et al. in 2012 proposed the concept of a Thermal Driven Electrochemical Generator, consisting in a *RED* unit coupled with a distillation column fed with ammonium bicarbonate solutions [18]. The authors experimentally proved the feasibility of the *RED* unit fed by NH_4HCO_3 to generate

electricity, achieving a maximum power density equal to 0.33W/m^2 of cell pair. Further experimental investigations related to the use of ammonium bicarbonate in *RED* units were reported by Kwon et al. in 2015 [19], who reported a maximum power density (1.45 W/m^2 of cell pair) doubled than the one achieved by Luo et al., and by Bevacqua et al. [20] in 2016, who reported the highest net power density so far achieved using such solutions (i.e. equal to 2.42W/m^2 of cell pair). However, none of these works focused on the experimental characterisation of the regeneration step, nor on the development of the integrated system.

Some other authors focused on the modelling analysis of *SGP-HE*. In 2007 McGinnis et al. theoretically investigated a closed loop configuration, named Osmotic Heat Engine (*OHE*)", consisting of a *PRO* unit coupled with a distillation column fed with ammonium bicarbonate solutions [21]. In 2014 Lin et al. carried out a theoretical study on *OHE* fed by NaCl solutions, in which *PRO* was coupled with a Membrane Distillation (*MD*) [22]. Theoretical estimations indicate that system efficiency could reach exergy efficiency of about 75-83% using low grade waste heat at 60°C.

Carati et al. [23] and Giacalone et al. [24] performed theoretical analysis to investigate the impact of different salt-water solutions on the performance of a *SGP-HE* constituted by a generic SGP unit and an evaporative regeneration unit, indicating how salts with high solubility and high activity coefficients at larger concentration can lead to the best theoretical performance of a *SGP-HE*.

Long et al. [25] and Micari et al. [26] performed a parametric study on hybrid RED-MD systems fed by NaCl solutions. The results have shown maximum exergy efficiency of about 16.5%, for optimal operating conditions. In 2017, Kim et al. presented a model to assess the performance of a *RED* unit fed by ammonium bicarbonate solutions for low-grade waste heat recovery [27]. Bevacqua et al. carried out a modelling analysis on *RED-HE* system operating with NH_4HCO_3. The *HE* proposed is constituted by a *RED* unit and thermal regeneration unit including an air-stripping column to restore the initial salinity gradient. The highest exergy efficiency reported was above 20% [28].

Recently, accurate analyses have shown that reverse electrodialysis – multi effect distillation heat engine (*RED-MED HE*) might achieve exergy efficiency ranging between 25-30% by using optimized membranes [29,30].

Despite the interesting results of theoretical analysis reported in the literature, no real demonstration of the process feasibility has been presented so far, due to the significant efforts required to design, construct and operate a fully integrated *RED-HE* system.

In the present work, for the first time in the literature, a fully operating prototype of a *RED-HE* operating with ammonium bicarbonate solutions has been designed, built and tested.
The proposed integrated prototype consists of: (i) a reverse electrodialysis unit, where salinity gradient from two ammonium bicarbonate solutions is converted into electricity; (ii) a regeneration unit composed of a vapour stripping column, where ammonia and carbon dioxide are desorbed from the dilute stream and a barometric condenser, where the stripped gases are re-absorbed in the concentrate stream, overall restoring the original salinity gradient. An extended experimental campaign has been carried out in order to demonstrate the feasibility of the process during long-run tests and to evaluate the effect of solutions concentrations and the main operating parameters on the system performance.

Method

Process description

The thermolytic *RED-HE* prototype consists of two units: (i) a *RED* unit where power is produced exploiting the salinity gradient between two ammonium bicarbonate solutions ("power unit") and (ii) a thermal regeneration unit where low-grade waste heat is used to restore the initial conditions of the two feed streams ("regeneration unit"). The concept scheme of the whole thermolytic *RED-HE* is reported in *figure 1*.

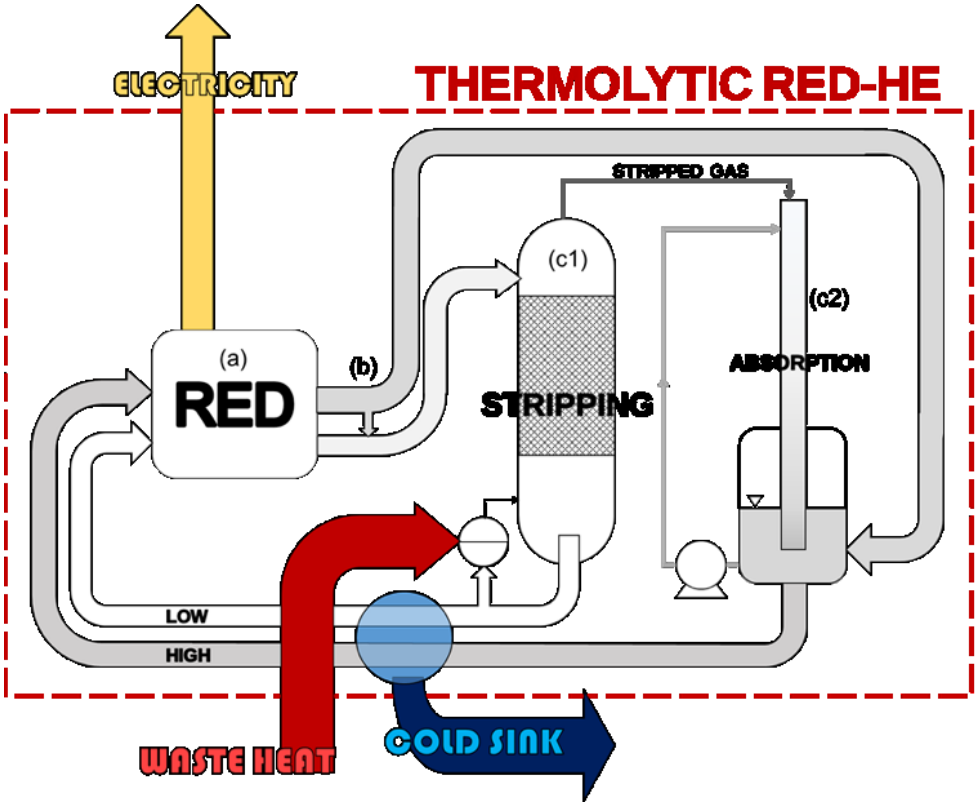

Figure 1. Concept scheme of the Thermolytic RED-HE. (a) Power unit; (b) water rebalancing; (c1) stripping of thermolytic salt; (c2) condensation/absorption of the gases.

The process steps can be described as follows:

(a) Power Unit. A dilute ammonium bicarbonate solution (*LOW*) and a concentrate ammonium bicarbonate solution (*HIGH*) are fed in a *RED* unit to convert their salinity gradient into electricity. As a result of the controlled mixing process, the flow-rate and composition of the two streams is altered: part of the salt from the *HIGH* solution is transferred to the *LOW* solution and, due to osmotic flux, water is transferred from the *LOW* solution to the *HIGH* solution. In order to restore the initial conditions of the two streams, salt and water have to be transferred in the opposite directions within the regeneration unit.

(b) Water rebalancing. Before entering the regeneration unit, a by-pass stream from the exhausted *HIGH* to the *LOW* stream restores the water content in the *LOW* loop, compensating for the water losses due to osmosis in the *RED* unit and evaporation in the stripping column. The mixing process represents a source of irreversibility, dissipating part of the chemical energy of the two streams and reducing the overall energy performance.

(c) Regeneration Unit. Solutions' regeneration is obtained in two steps: (c1) stripping of thermolytic salts from the LOW solution and (c2) condensation-absorption of the gases in the HIGH solution. After the water rebalancing, the *LOW* stream is preheated and fed on the top of the stripping column, where it is distributed on the packing material and put in contact with the rising vapour. The stripping vapour is produced in a reboiler placed on the bottom of the column, where part of the solution is vaporized. The mass and enthalpy exchanges between vapour and solution promotes the salt degradation and the stripping of ammonia (NH_3) and carbon dioxide (CO_2) reducing the ions (i.e. NH_4^+, HCO_3^-, CO_3^{2-} and $NH_2CO_2^-$) concentration in solution. The regenerated *LOW* solution exiting from the reboiler is cooled down to 25°C. The main chemical equilibrium reactions occurring in ammonium bicarbonate-water solutions are:

$$NH_4HCO_3 \leftrightarrow NH_4^+ + HCO_3^- \quad (1)$$

$$NH_4^+ + OH^- \leftrightarrow NH_3 + H_2O \quad (2)$$

$$HCO_3^- + H_3O^+ \leftrightarrow CO_2 + 2H_2O \quad (3)$$

$$NH_3 + HCO_3^- \leftrightarrow NH_2COO^- + H_2O \quad (4)$$

$$HCO_3^- + H_2O \leftrightarrow CO_3^{2-} + H_3O^+ \quad (5)$$

The stripped gases reach the barometric condenser, connected with the top of the stripping column. Before entering the barometric column, these gases are cooled down to 25°C in order to partially condense water and ammonia and facilitate the CO_2-NH_3 absorption process. The barometric condenser produces the vacuum needed to operate the stripping column at low temperature (<100°C) and promotes the condensation and absorption of the stripped gases in the *HIGH* solution. It is operated by recirculating a cold stream from the bottom to the top of the column, where it is mixed with the *HIGH* solution exiting from the RED unit. The regenerated *HIGH* solution exiting from the bottom of the barometric condenser is eventually recirculated to the RED unit.

Prototype description

A schematic diagram of the prototype is reported in *figure 2*. The *RED* unit provided by REDstack BV (The Netherlands) consists of 50 cell pairs with an active membrane area of 0.1x0.44m^2 (1). Each cell pair consists of one cation and one anion exchange membrane (Type 10 - Fujifilm Manufacturing Europe BV -The Netherlands), and two compartments, i.e. a dilute (*LOW*) and a

concentrate (*HIGH*) compartment, equipped with woven spacers of 155 micron (Deukum GmbH, Germany).

Magnetic gear pumps (fluid-o-tech FG204) circulate the feed solutions to the unit. An electrodic rinse solution with $K_3Fe(CN)_6/K_4Fe(CN)_6$ redox couple is recirculated in the electrodes in order to convert the ionic current into an electric current. In order to minimize osmotic and diffusive fluxes from/to electrodic compartments a proper supporting electrolyte (NH_4HCO_3) was added in the electrode rinse solution. Moreover, very permselective end-membranes (Fumasep F-10150-PF), Fumatech GmbH (Germany), were used to further minimize salt passage.

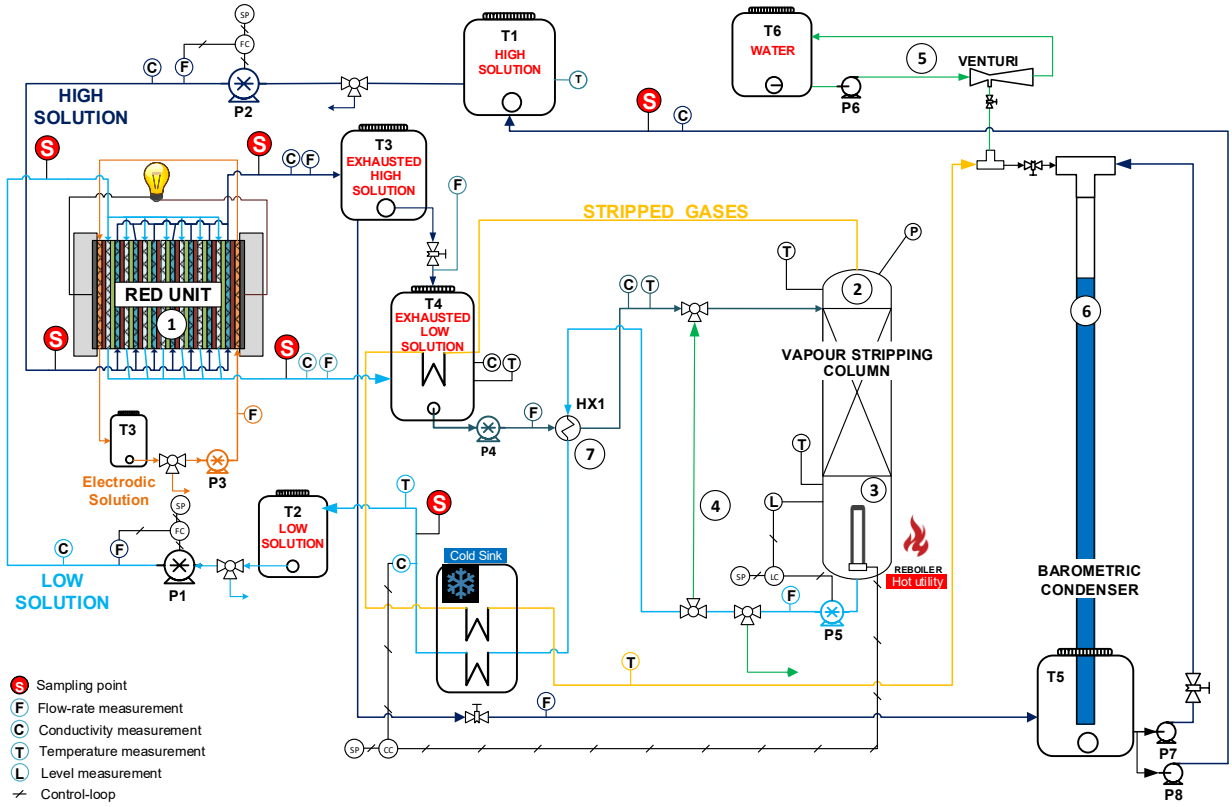

Figure 2 Simplified P&I diagram of the thermolytic RED-HE. Main components: (1) RED unit; (2) stripping column; (3) reboiler; (4) auxiliary circuit; (5) Venturi ejectors; (6) barometric condenser; (7) thermal integration heat exchanger; (S) sampling points.

The vapour stripping column (2) consists of a Plexiglas tube with an internal diameter of 50 mm filled with a structured packing material (KOCH-Glitsch FLEXIPAC® 700Y). The packing height is 1.6 m. The bottom of the column is connected to a reboiler (3) where the stripping vapour is generated. For the purpose of the present work, the external energy input is a low-temperature

194 electrical resistance, which replaces the use of waste heat. The heat provided by the electrical
195 resistance is set regulating the intensity of the electrical current supplied. A T-type thermocouple is
196 used to measure the temperature of the solution in the reboiler. On the top of the column, a liquid
197 distributor is used to sprinkle the incoming *LOW* solution on the packing material. The top of the
198 column is connected to an absolute pressure transducer (VEGA - VEGAbar 14) and a T-type
199 thermocouple. The barometric condenser consists in a 15m tube (ID ½') with the bottom end
200 submerged in the *HIGH solution tank* (6). A double-pipe hair-pin heat-exchanger is used for thermal
201 integration in order to recover part of the heat from the *LOW* regenerated solution exiting from the
202 reboiler and to preheat the solution fed to the vapour stripping column (7). It consists of a stainless
203 steel AISI 316 tube (ID 6mm, thickness 1.5mm) inserted in a Plexiglas tube (ID 12mm, thickness
204 2mm), with the cold stream flowing in the annular section.

205 The conductivity, temperature and flow-rate of the main streams in both the RED and REG units are
206 monitored by on-line sensors (C), (T) and (F). For cross-checking conductivity and temperature
207 values, also sampling points were used (S).

208 Control-loops were implemented in the prototype to control the RED unit inlet flow-rates, the
209 regenerated dilute solution from the column (by acting on the heat supplied to the reboiler) and the
210 liquid level in the reboiler (by acting on the liquid outlet flow rate).

211 During the start-up phase only, auxiliary circuits are used to recirculate hot solution from the reboiler
212 to the top of the column in order to heat-up the packing material (4) and to evacuate air using an
213 auxiliary Venturi ejector vacuum system (5). A picture of the prototype system is reported in *figure*
214 *3.*

215 **Experimental procedure**

216 The two feed solutions are prepared dissolving anhydrous ammonium bicarbonate salt (Carlo Erba®
217 purity >99.5%) into deionized water. The electrode rinse solution is prepared dissolving 0.1mol/l of
218 $K_3Fe(CN)_6$ and 0.1mol/l $K_4Fe(CN)_6 \cdot 3H2O$ in deionized water and adding ammonium bicarbonate at
219 a concentration equal to the average of the two feed solutions.
220 An experimental calibration was performed in order to relate the measured conductivity (at 25°C) to
221 the concentration of dissolved salt by the equation (6):

$$\lambda = \Lambda \cdot C \quad (6)$$

where λ is the solution conductivity (mS/cm), Λ is the specific molar conductivity (mS $cm^{-1}mol^{-1}l$)) and C is the molar concentration. The specific conductivity (mS $cm^{-1}mol^{-1}l$)) of ammonium bicarbonate solution is evaluated according to:

$$\Lambda = \Lambda_0 - \frac{A_\Lambda C^{1/2}}{1 + B_\Lambda C^{1/2}} - C_\Lambda C \quad (7)$$

where Λ_0 is the equivalent conductivity of salt at infinite dilution, A_Λ, B_Λ and C_Λ are fitting parameters, and C is the molar concentration. The fitting coefficients for NH_4HCO_3 at 298K have been obtained by fitting experimental data leading to: Λ_0 = 101.88 A_Λ = 30.32, B_Λ = C_Λ = 0. In particular, both literature data [31] and original experiments were used in order to double check the consistency of the equation with the real behaviour of solutions.

Although the chemical equilibria occurring in ammonium bicarbonate aqueous solutions lead to the formation of different ions, from the main ones as NH_4^+ and HCO_3^-, to the less abundant CO_3^{2-} and $NH_2CO_2^-$ (as reported in eqs. 1-5), the stable operating conditions of the regeneration process and the minimisation of CO_2 and NH_3 release (assessed in the long-run tests presented in the next section), have allowed a reliable use of the above conductivity-concentration relation.

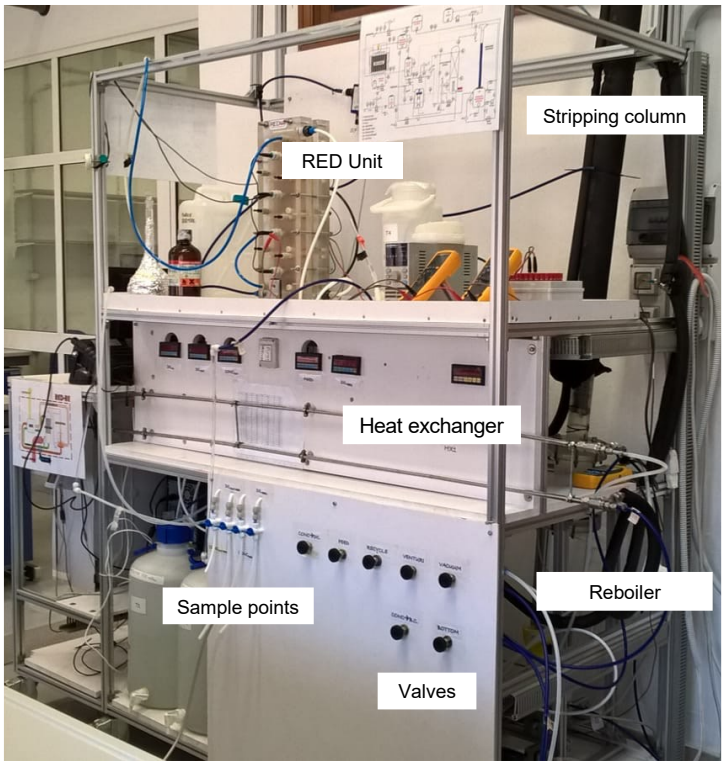

Figure 3 The thermolytic RED-HE prototype.

For the purpose of this work, the inlet flow-rates in the *RED* unit are fixed equal to 0.2 l/min (corresponding to a *RED* channels' velocity of 0.5 cm/s) in all cases. This value gives a good compromise between *RED* unit and vapour stripping column operability. Furthermore, in a previous theoretical investigation, it was shown that the global system efficiency is maximized by adopting low solution velocities in the RED unit in order to increase the residence time and the power yield [32]. Polarisation phenomena are not relevant in RED units operating in these conditions thanks to the high solution concentration used [33].

During continuous operation, the *RED* unit is connected to a fixed external load. The value of the external resistance is chosen in order to operate around the maximum power density condition. However, during the performed experiments, the characteristic power-output behaviour was also assessed at different operating times in order to analyse possible variations in the *RED* unit performance. Thus, the value of external resistance was varied from open-circuit (*OC)* to short-circuit (*SC*) condition, measuring both stack voltage (V_{stack}) and current (I_{stack}) using two multimeters (FLUKE 175). The electric power generated by the *RED* (P_{RED}) unit is given by:

$$P_{RED} = I_{STACK} \cdot V_{STACK} \quad (8)$$

The performance of the RED units is typically evaluated also in terms of maximum power density, i.e. the maximum power generated per unit of cell pair:

$$P_{d,\max} = \frac{P_{RED,\max}}{A_m N_{cp}} \quad (9)$$

where $P_{RED,max}$ is the maximum power produced by the *RED* unit (for ideal stacks with short channels, corresponding to the condition V=OCV/2), A_m is the active area of one membrane (i.e. 0.1x0.44m^2) and N_{cp} is the number of cell pairs (i.e. N_{cp} =50).

The solutions exiting from the regeneration unit are cooled down in the range 23-27°C in order to control the operating temperature of the RED unit. Indeed, higher operative temperatures may result in an increase in the RED power output but lead to a risky condition of gas bubble formation in the stack due to salt degradation.

The pressure at the top of the stripping column varies in the range 0.41–0.56bar, while the reboiler temperature is in the range of 78–85°C. A start-up period of about 30 minutes is required in order to reach a steady-state condition in the stripping column. The thermal duty of the reboiler is a growing function of the inlet solution concentration. In all investigated cases, the thermal duty is modulated in order to restore the original concentration of the solution fed to the *RED* unit. A solid-state relay was used in order to regulate the current provided to the heater (in the range 0 to 10 A) by applying a voltage input in the range 0-10V. The voltage provided to the external heater was maintained equal to the main voltage (about 226V). Thus, thermal duty provided in the reboiler was calculated by measuring both electrical voltage and current by a True RMS multimeter. The specific thermal consumption (*STC*) is defined as the ratio between the electrical power provided to the reboiler (or the thermal duty *TD*) and the flowrate entering in the stripping column *($F_{in,REG}$):*

$$STC = \frac{TD}{F_{in,REG}} \quad (10)$$

The prototype was tested under long run operations for more than 50 hours, aiming to assess the robustness of the process under constant external load conditions. In particular, the operations were carried-out in different days (three or four days) by cycling always the same solutions within the

279 units. In the first days, the prototype was continuously operated for a duration ranging from 8 to 12
280 hours. Then it was turned-off and started-up again in the following day, in order to simulate possible
281 on/off operating cycles of the system when used in "energy storage" mode. Finally, in last day the
282 prototype was operated for at least 24 h continuously.

283 In order to evaluate operational stability on a relevant time-scale, a non-dimensional parameter was
284 defined, namely N_{RED}^{C} , as the ratio between the test duration and the residence time of solution within
285 the RED unit:

286 $$N_{RED}^{C} = \frac{t_{test}}{t_{RED}} \quad (11)$$

287 where

288 • t_{RED} (residence time in the RED unit) is the ratio between liquid hold-up in the channels (i.e.
289 0.28 l) and flow rate (i.e. 0.2 l/min);

290 • t_{test} is the duration of the long run test (in minutes).

291 In particular, N_{RED}^{C} can be seen as the number of cycles that the feed solutions undergo during closed-
292 loop operation within the *RED* unit Values of t_{RED} close to 2700 have been reached in the present
293 investigation with time duration of the long-run test up to 55 hours.

294 Also for the regeneration unit, a non-dimensional parameter (i.e. N_{REG}^{C}) was introduced to evaluate
295 the number of cycles, which the *LOW* solution (being regenerated) undergoes during closed-loop
296 operation in the packing material of the stripping column. This parameter is defined as:

297 $$N_{REG}^{C} = \frac{t_{test}}{t_{REG}} \quad (12)$$

298 where

299 • t_{REG} is the ratio between the liquid hold-up in the stripping column (estimated as 0.10 of the
300 column volume) and the flow rate (i.e. 0.23 l/min) entering the unit;

301 It is worth defining here also some important thermodynamic figures of merit, which help
302 characterising the system performance. In particular, the maximum amount of power to be harvested
303 from the mixing of solutions at different concentration is given by the Gibbs free power of mixing (

304 $\Delta\dot{G}_{mix}$), evaluated as the Gibbs free power of the resulting solution ($\dot{G}_{mix}$) minus the one of the two
305 original streams ($\dot{G}_H + \dot{G}_L$):

306 $$\Delta\dot{G}_{mix} = \dot{G}_{mix} - \dot{G}_H - \dot{G}_L \quad (13)$$

307 The Gibbs free power of the generic i^{th} stream ( ) is evaluated considering both water and salt
308 contributions:

309 $$\dot{G}_i = \dot{n}_i\mu_i = \dot{n}_{salt,i}\mu_{salt,i} + \dot{n}_{water,i}\mu_{water,i} \quad (14)$$

310 where $\mu_{salt,i}$ and $\mu_{water,i}$ are the chemical potential of salt and water, respectively,[34,35] and
311 the molar flow rates (mol/s) of salt and water in the i^{th} stream. The ratio between experimental
312 electrical power produced and the Gibbs free power of mixing is the thermodynamic yield (Y) of the
313 process:

314 $$Y = \frac{P_{RED}}{\Delta\dot{G}_{mix}} \quad (15)$$

315 The RED exergy efficiency ($\eta_{ex,RED}$) represents the fraction of the consumed chemical exergy
316 converted into electrical power within the *RED* unit, and is defined as[29]:

317 $$\eta_{ex,RED} = \frac{P_{RED}}{\left(\dot{G}_{H,in} + \dot{G}_{L,in}\right) - \left(\dot{G}_{H,out} + \dot{G}_{L,out}\right)} \quad (16)$$

318 The thermal efficiency of the system (η_{th}) is defined as the ratio of the electrical power generated (
319 P_{RED}) by the RED unit and the thermal duty of the stripping column according to:

320 $$\eta_{th} = \frac{P_{RED}}{TD} \quad (17)$$

321 Finally, the exergy efficiency of the system (η_{ex}) is the ratio between the thermal efficiency of the
322 investigated heat engine (η_{th}) and the efficiency of an ideal Carnot engine (η_C), operating in the same
323 range of temperature:

324 $$\eta_{ex} = \frac{\eta_{th}}{\eta_C} \quad (18)$$

All the performance indicators refer to gross values of generated power, not considering the power required to operate the prototype. As a qualitative indication, pumping losses in an optimised RED unit are typically in the range of 10-20% [36] of the generated power. Similar values are estimated for the regeneration unit under properly optimised conditions.

Results & Discussion

Long-run tests were carried out with 4 different salinity gradients at the inlet of the RED unit (see *Table 1*), analysing the behaviour of the system in terms of conductivity of the solutions and system's performance indicators, namely: power density, specific thermal consumption and exergy efficiency. As reported in *Table 1*, the long-run tests were performed for 8 h, for cases A and C, and up to 55 h, for cases B and D. For these latter cases, the operation was extended to several days, initially with intermittent functioning (8-12 hours of operation alternated with 12-16 hours of stop) in order to simulate the use as "energy storage" system, and a final continuous run, in which the prototype was continuously operated for more than 24 h.

Table 1. Operating conditions of the four investigated cases.

	HIGH SOLUTION	LOW SOLUTION	DURATION	COLUMN CONDITIONS	
case	**Molarity [M] (λ_{av} [mS/cm])**	**Molarity [M] (λ_{av} [mS/cm])**	**Time [h] (N^{C}_{RED})**	**P_{TOP} [bar]**	**T_{BOTTOM} [°C]**
(A)	0.6 (45.9)	0.05 (4.9)	8 (360)	0.40	77.0
(B)	1.0 (72.8)	0.052 (5.2)	55 (2700)	0.43	78.0
(C)	1.45 (94.8)	0.05 (4.8)	9 (400)	0.49	81.7
(D)	1.9 (114)	0.052 (5.2)	55 (2700)	0.55	84.5

Analysis of system stability in long-run operation

The t-RED HE prototype was tested in order to analyse the behaviour and stability of all components during long-run tests. The time variation of the conductivity of the solutions at the inlet and at the outlet of the *RED* unit working close to maximum power density condition (external load resistance

equal to 1.2Ω), is reported in *figures 4a* and c for the cases B (i.e. 1.0M-0.05M) and D (i.e. 1.9M-0.05M), respectively, as a function of N_{RED}^{C} and operating time.

In particular, referring to case D (*fig. 4c*), the concentration of the "*HIGH*" inlet solution is reduced from 1.9M (i.e. 114 mS/cm at 25°C) to 1.43M (i.e. 93.8mS/cm at 25°C), conversely the "*LOW*" solution concentration is increased almost sevenfold from 0.05M (i.e. 5.2mS/cm at 25°C) to 0.38M (i.e. 31.7mS/cm at 25°C). After the water rebalancing step (see *section 2.1*), which produces a further increase of the *LOW* concentration from 0.38M to 0.54M (i.e. 42.6mS/cm at 25°C), the initial concentrations were eventually restored in the regeneration unit, where the thermolytic salt decomposes and is removed as gas ammonia and carbon dioxide. The stripped gases are then absorbed in the *HIGH* solution within the barometric condenser. The time variation of regenerated solutions conductivity is reported in *figures 4b* and *4d* for the cases B (i.e. 1.0M-0.05M) and D (i.e. 1.9M-0.05M), respectively. In particular, referring to case D (*fig. 4d)*, the LOW solution conductivity is reduced from 0.54 M (i.e. 42.6mS/cm at 25°C) to 0.05M (i.e. 5.2mS/cm at 25°C), while the *HIGH* solution conductivity is increased from 1.43M (i.e. 93.8mS/cm at 25°C) to 1.9M (i.e. 114mS/cm at 25°C), thus restoring the original salinity gradient. Similar consideration can be done for the results reported in *figures 4a* and 4b for the case B.

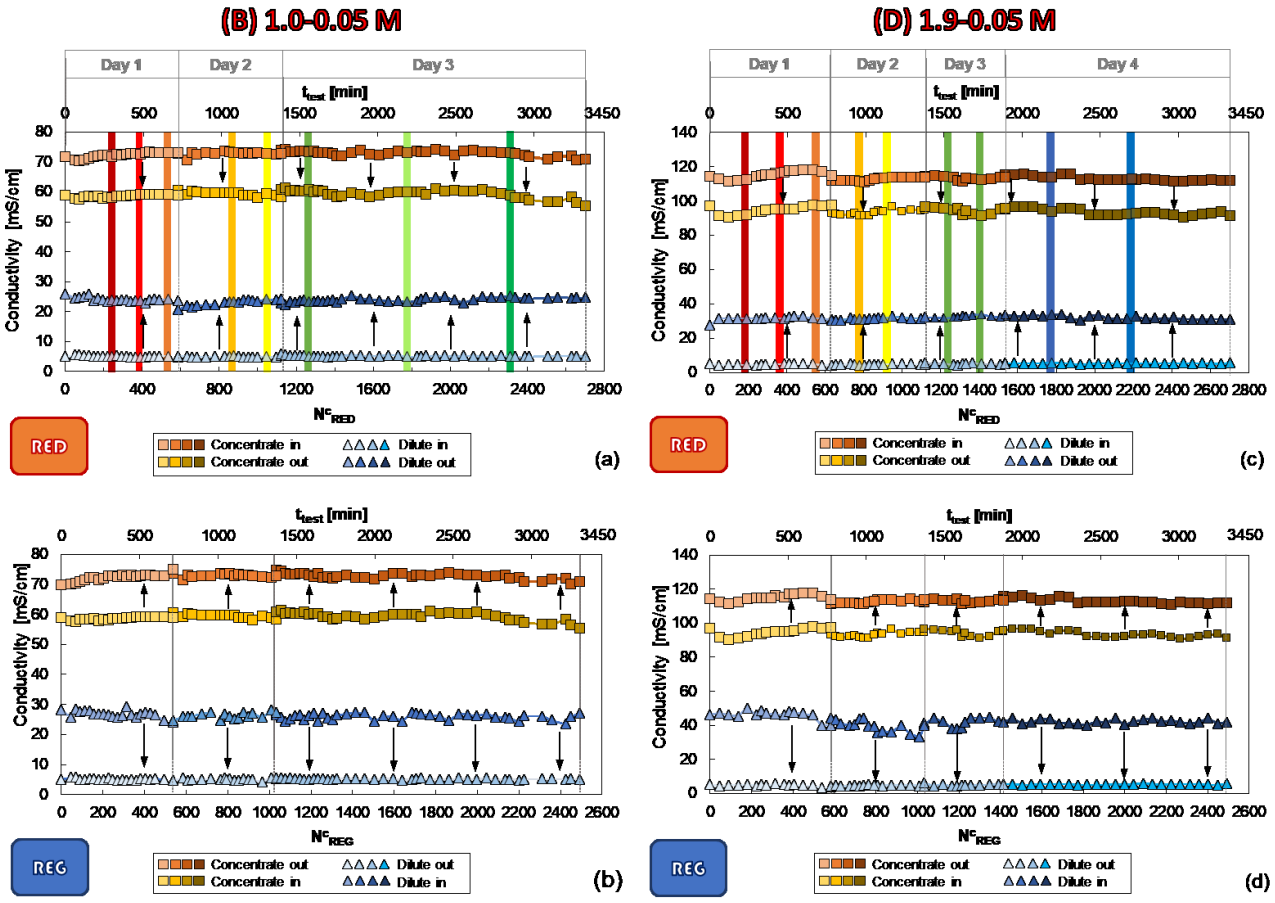

Figure 4 Time variation of inlet/outlet conductivity of the solutions in the RED unit (a and c) and in the regeneration unit (b and d) for the cases D and B of table 1, respectively. Coloured vertical bars in figure a and c indicate when power density measurements were performed as reported in figure 6.

The stability of concentration values over time clearly indicates the robustness of the system, both in continuous operation and also in intermittent operations (when the prototype was stopped and the regenerated solutions were stored during 12-16 hours in the buffer tanks), highlighting the potential of the RED HE to be used for energy storage applications.

During the test, the system performance in terms of power density, Specific Thermal Consumption and exergy efficiency were monitored. Relevant results are reported in *figure 5* for cases B and D. In all cases, the power density increases of about 10% in the first 1-2 hours of operation then achieving a steady state condition. This behaviour can be attributed to the membranes' stabilisation and the relevant reduction of the RED unit electrical resistance. Then, only very small deviations (~5%) from the average value are observed during the 55 hours or 2700 cycles (N^C_{RED}) of operation. The average

values of $P_{d,max}$ is about 1.5 W/m^2 for the case D (1.9M-0.05M), and 0.9W/m^2 for the case B (1 M-0.05M). As expected, the increase of the RED unit *HIGH* solution concentration from 1.0M to 1.9M results into an increase of the outlet concentration of the *LOW* solution. In fact, the higher salinity gradient available leads to an increase of both the migrative flux across the IEMs (contributing to increase the power generated) and the uncontrolled mixing phenomena (i.e. diffusive and osmotic salt and water fluxes, respectively).

This also leads to larger power requirements in the regeneration step. In particular, the average *STC* is equal to 93 kWh/m^3 for case B and 110 kWh/m^3 for case D (*fig. 5c* and *d*). Also for the *STC* just small deviations (~5%) are observed in the 55 hours of operations (i.e. in 2500 N_{REG}^{C} cycles).

The exergy efficiency of the system during the long run tests is reported in *Figure 5e* and *f*. In particular, the average exergy efficiency is equal to 1.1% for case D and 0.8% for case B, with small oscillations derived by the trends of P_d and *STC*.

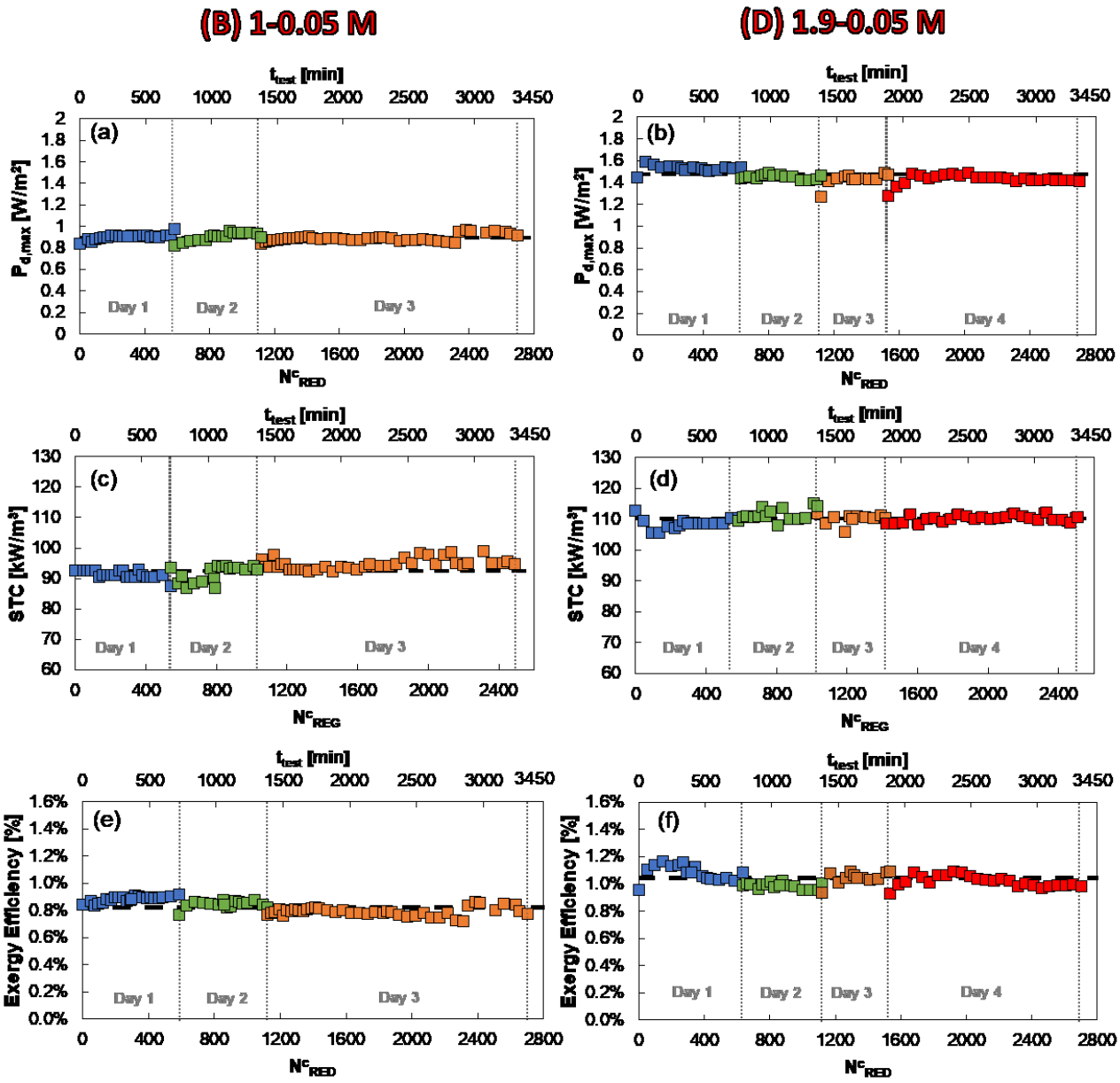

385

Figure 5 Time variation of power density ($P_{d,max}$), Specific Thermal Consumption (STC) and exergy efficiency of the system for the cases B (i.e. figure a, c, and e) and D (i.e. figure b, d, and f) of table 1.

386

387 **RED power generation in the four salinity gradient scenarios**

388 RED power generation performance is typically characterised using the so called "polarisation
389 curves", consisting in a plot of the measured stack electrical voltage (V_{stack}) and generated power
390 density (P_d) as a function of the electrical current (I_{stack}) and voltage (V_{stack}), respectively.

Experimental results for all different salinity gradient scenarios are reported in *figures 6a* and *6b* for comparison purposes. Note that for cases A and C results refer to one day (8-9 hours) of continuous operations, while for cases B and D, they refer to different sampling times in the 3 or 4 days of operation, as indicated by the coloured rectangles in *figures 4a* and *4c*.

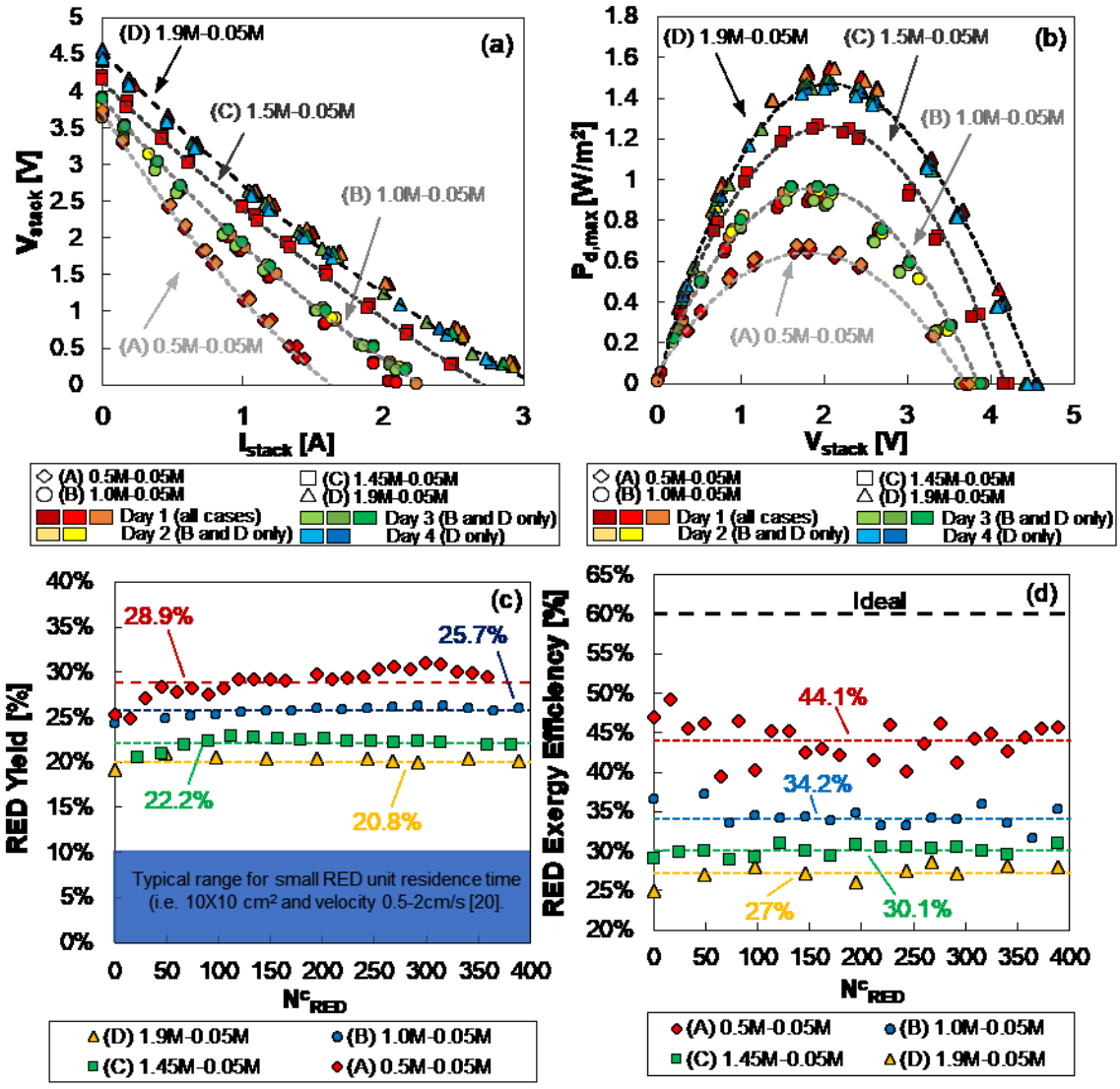

Figure 6 (a) Stack voltage vs stack current and (b) electrical power density vs stack voltage generated by the RED unit. Different series report measurements performed at different number of cycles in the RED unit. (c) Thermodynamic yield vs number of RED unit cycles: measured values and range typically reported in the literature for smaller laboratory stacks[20]. (d) RED Exergy conversion efficiency vs number of RED unit cycles: experimental measured values and theoretical value for an "ideal membrane stack" (unitary permselectivity, null water and salt permeability). Experimental results refer to test cases (A, B, C, D) reported in Table 1.

The first important evidence is the stable behaviour of the power generation unit in all cases, which leads to a very good reproducibility of all power density curves (*figure 6b*).

Another interesting finding is the non-ohmic behaviour of the stack, as denoted by the non-linear relationship between V_{stack} and I_{stack} (*figure 6a*). In fact, as a result of the increasing electrical current, the internal stack resistance is reduced due to the increase in the *LOW* solution conductivity. This is identified by the deviation of the voltage/current curve from the linear ohmic trend (whose slope identifies the internal stack resistance), which indicates a continuous decrease in the stack resistance. This effect is made evident thanks to the high residence times (i.e., low velocities and long channels) adopted in this study. Also for this reason, the maximum power density generated in the *RED* unit (~1.5 W/m^2), when using ammonium bicarbonate solutions at 1.9M and 0.05M, is lower than the highest values reported so far in the literature (i.e., 2.42 W/m^2) [20].

On the other side, the adoption of higher residence times guarantees a better exploitation of the available salinity gradient. An average yield of almost 30% is obtained in the case A, which goes down when increasing the salinity gradient reaching about 21% in the case D (*Figure 7a*). These values are about fivefold the values obtainable with small laboratory *RED* units as reported in the literature. The increase of HIGH solution concentration reduces the yield of the process due to the larger available Gibbs free energy to be exploited (longer residence time could be used), but also to the increase of the uncontrolled mixing phenomena [35], as also denoted by the lower xergy efficiency. This latter, in particular, is decreased from 44% to 27% by increasing the HIGH solution concentration from 0.5M to 1.9M (*Figure 7b*). Interestingly, the exergy efficiency of the system compares very well with the maximum value obtainable in a stack provided with ideal membranes (i.e. unitary permselectivity, null water and salt permeability) operating at the same conditions (close to 60%). All these findings show a good exploitation of the available salinity gradient.

Influence of adopted salinity gradients on the overall prototype performances.

An overall comparison of the system performance indicators is reported in *Figure 8* where the average values of power density, specific thermal power consumption and exergy efficiency during first 8 hours of operation are plotted as a function of the HIGH solution concentration. As expected, the power density in the RED unit increases when the *HIGH* solution concentration increases, due to the larger available driving force. In particular, the maximum power density of 1.5W/m^2 is observed for

the case 1.9-0.05M (D). It decreases to (i) 1.3W/m^2 for the case 1.45M-0.05M (C), (ii) 0.9W/m^2 for the case 1.0M-0.05M (B) and (iii) 0.63W/m^2 for the case 0.5M-0.05M (A). On the other hand, the higher the *HIGH* solution concentration, the higher the specific thermal power consumption in the vapour stripping column (i.e. the ratio between the *Thermal Duty* and the inlet flow rate) to regenerate the solutions, ranging from 77 kWh/m^3 to 110 kWh/m^3 moving from case A to D.

However, the increase of power output with the *HIGH* solution concentration has a prevailing effect, thus resulting into the highest exergy efficiency value of 1.1%, observed in the case of the highest driving force considered (i.e. 1.9M-0.05M).

Under the investigated conditions, a further increase of the HIGH solution concentration would not result in a relevant increase of the global exergy efficiency. In fact, the concentration increase would lead to a larger amount of gases released in the stripping column, which would increase the operating pressure of the system and result in a higher regeneration temperature (see *table 1*). Thus, despite the likely increase of the thermal efficiency, the larger heat-source temperature would produce an increase of the maximum theoretical Carnot efficiency, thus maintaining the exergy efficiency at almost constant values. On the other side, operating at HIGH concentrations close to salt saturation would dramatically increase the risk of local salt precipitation in the HIGH loop regeneration phase, thus dramatically affecting the potential for long-term stable operation of the system.

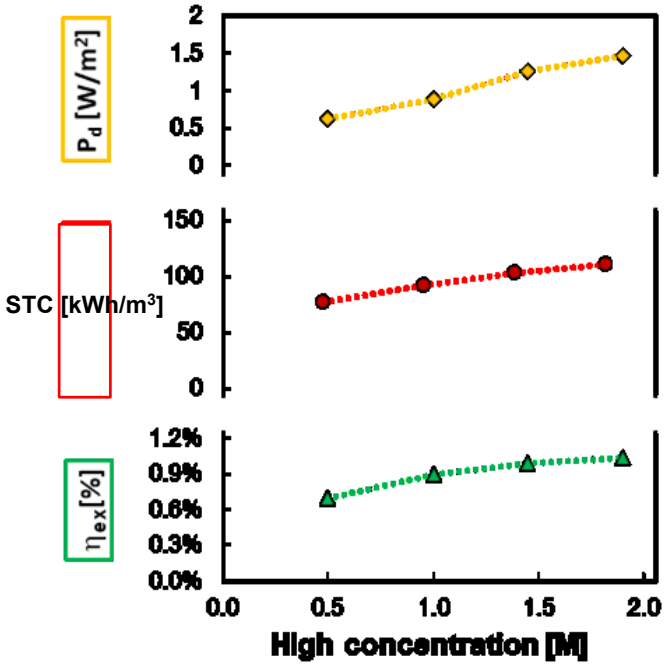

Figure 8 Average values (obtained in the first 8 hours of operation) of maximum power density ($P_{d,max}$), specific thermal consumption (STC) and exergy efficiency (η_{ex}) of the thermolytic RED-HE as a function of the High solution concentration. Experimental results refer to test cases reported in Table 1.

Conclusions

Reverse electrodialysis in closed-loop (RED heat engine) is a novel technology to convert low-grade heat into electricity. Promising performance have been recently envisaged by modelling activities and reported in the literature for several combinations of regeneration technologies, indicating achievable exergy efficiency in the order of 25-30%. In the present work, the first experimental assessment of a thermolytic *RED* Heat Engine (t-RED HE) is presented. The first t-RED HE prototype was designed and built in order to investigate the feasibility of the process. It consists of a RED unit fed with ammonium bicarbonate solutions, coupled with a vapour-stripping column operated at temperatures well below 90°C. The system stability and performance were analysed under different operating conditions via long-run tests. The highest values of yield and exergy conversion efficiency have been reported for the first time in the literature for *RED* units operating with thermolytic solutions. The highest exergy efficiency measured was equal to 1.1% for the case of 1.9M-0.05M ammonium bicarbonate solutions. The results collected indicate good stability of the process over operational times up to 55 hours, in terms of solutions properties, power generation and thermal consumption. Moreover, the possibility to adopt the system for energy storage applications has been assessed under intermittent operations performed in different days.

Theoretical analyses presented in other works suggest that large room for improvements still exists, including the development of enhanced membranes suitably tailored to operate with ammonium bicarbonate solutions and the design of a more efficient regeneration unit adopting thermal integration with multi-column arrangement.

The successful implementation of the first t-RED HE poses the first stone to move Loeb's idea from theory to reality.

Acknowledgements

This work has been performed within the RED-Heat-to-Power project (Conversion of Low-Grade Heat to Power through closed loop Reverse Electro-Dialysis), funded by EU within the H2020 research & innovation programme, grant agreement No. 640667. www.red-heat-to-power.eu.

The authors are thankful to REDstack BV for providing the RED unit, Fujifilm Manufacturing Europe BV for providing IEMs membranes, Koch-Glitsch for providing the structured packing material of the stripping column.

We are also deeply grateful to Mr. Giuseppe Fanale for his essential support for the construction and commissioning of the prototype.

References

[1] Department of Energy, Waste Heat Recovery: Technology and Opportunities in U.S. Industry, (2008). https://www1.eere.energy.gov/manufacturing/intensiveprocesses/pdfs/waste_heat_recovery.pdf.

[2] D.B. Gingerich, M.S. Mauter, Quantity, Quality, and Availability of Waste Heat from United States Thermal Power Generation, Environ. Sci. Technol. 49 (2015) 8297–8306. doi:10.1021/es5060989.

[3] R. Law, A. Harvey, D. Reay, A knowledge-based system for low-grade waste heat recovery in the process industries, 94 (2016) 590–599. doi:10.1016/j.applthermaleng.2015.10.103.

[4] M. Papapetrou, G. Kosmadakis, A. Cipollina, U. LaCommare, G. Micalea, Industrial waste heat: Estimation of the technically available resource in the EU per industrial sector, temperature level and country, Appl. Therm. Eng. 138 (2018) 207–216. doi:10.1016/j.applthermaleng.2018.04.043.

[5] M.A. Khatita, T.S. Ahmed, F.H. Ashour, I.M. Ismail, Power generation using waste heat recovery by organic Rankine cycle in oil and gas sector in Egypt: A case study, Energy. 64 (2014) 462–472. doi:10.1016/j.energy.2013.11.011.

[6] Y. Wang, Q. Tang, M. Wang, X. Feng, Thermodynamic performance comparison between ORC and Kalina cycles for multi-stream waste heat recovery, Energy Convers. Manag. 143 (2017) 482–492. doi:10.1016/j.enconman.2017.04.026.

[7] M. Rahimi, A.P. Straub, F. Zhang, X. Zhu, M. Elimelech, C.A. Gorski, B.E. Logan, Emerging electrochemical and membrane-based systems to convert low-grade heat to electricity, Energy Environ. Sci. 11 (2018) 276–285. doi:10.1039/c7ee03026f.

[8] O. Bubnova, X. Crispin, Towards polymer-based organic thermoelectric generators, Energy Environ. Sci. 5 (2012) 9345–9362. doi:10.1039/c2ee22777k.

[9] M. Zebarjadi, K. Esfarjani, M.S. Dresselhaus, Z.F. Ren, G. Chen, Perspectives on thermoelectrics:

From fundamentals to device applications, Energy Environ. Sci. 5 (2012) 5147–5162. doi:10.1039/c1ee02497c.

[10] J.S. Jadhao, D.G. Thombare, Review on Exhaust Gas Heat Recovery for I.C. Engine, Certif. Int. J. Eng. Innov. Technol. 9001 (2008) 2277–3754. http://www.ijeit.com/vol 2/Issue 12/IJEIT1412201306_18.pdf.

[11] J. Karthauser, Energy generation from Waste Heat using the Carbon Carrier Thermodynamic Cycle, United States Patent Application 20160201521, 2016.

[12] F. Zhang, J. Liu, W. Yang, B.E. Logan, A thermally regenerative ammonia-based battery for efficient harvesting of low-grade thermal energy as electrical power, Energy Environ. Sci. 8 (2015) 343–349. doi:10.1039/c4ee02824d.

[13] R.E. Pattle, Production of Electric Power by mixing Fresh and Salt Water in the Hydroelectric Pile, Nature. 174 (1954) 660–660. doi:10.1038/174660a0.

[14] B.E. Logan, M. Elimelech, Membrane-based processes for sustainable power generation using water, Nature. 488 (2012) 313–319. doi:10.1038/nature11477.

[15] R.A. Neff, Solvent Extractor, US Patent 3130156, 1964.

[16] S. Loeb, Method and apparatus for generating power utilizing Pressure-Retarded-Osmosis, US Patent 3906250, 1974.

[17] S. Loeb, Method and apparatus for generating power utilizing reverse electrodialysis, US4171409A, 1979.

[18] X. Luo, X. Cao, Y. Mo, K. Xiao, X. Zhang, P. Liang, X. Huang, Power generation by coupling reverse electrodialysis and ammonium bicarbonate: Implication for recovery of waste heat, Electrochem. Commun. 19 (2012) 25–28. doi:10.1016/j.elecom.2012.03.004.

[19] K. Kwon, B.H. Park, D.H. Kim, D. Kim, Parametric study of reverse electrodialysis using ammonium bicarbonate solution for low-grade waste heat recovery, Energy Convers. Manag. 103 (2015) 104–110. doi:10.1016/j.enconman.2015.06.051.

[20] M. Bevacqua, A. Carubia, A. Cipollina, A. Tamburini, M. Tedesco, G. Micale, Performance of a RED system with ammonium hydrogen carbonate solutions, Desalin. Water Treat. 57 (2016) 23007–23018. doi:10.1080/19443994.2015.1126410.

[21] R.L. McGinnis, J.R. McCutcheon, M. Elimelech, A novel ammonia–carbon dioxide osmotic heat engine for power generation, J. Memb. Sci. 305 (2007) 13–19. doi:10.1016/j.memsci.2007.08.027.

[22] S. Lin, N.Y. Yip, T.Y. Cath, C.O. Osuji, M. Elimelech, Hybrid Pressure Retarded Osmosis–Membrane Distillation System for Power Generation from Low-Grade Heat: Thermodynamic Analysis and Energy Efficiency, Environ. Sci. Technol. 48 (2014) 5306–5313. doi:10.1021/es405173b.

534 [23] A. Carati, M. Marino, D. Brogioli, Thermodynamic study of a distiller-electrochemical cell system for
535 energy production from low temperature heat sources, Energy. 93 (2015) 984–993.
536 doi:10.1016/j.energy.2015.09.108.
537 [24] F. Giacalone, C. Olkis, G. Santori, A. Cipollina, S. Brandani, G. Micale, Novel solutions for closed-
538 loop reverse electrodialysis: Thermodynamic characterisation and perspective analysis, Energy. 166
539 (2019) 674–689. doi:10.1016/j.energy.2018.10.049.
540 [25] R. Long, B. Li, Z. Liu, W. Liu, Hybrid membrane distillation-reverse electrodialysis electricity
541 generation system to harvest low-grade thermal energy, J. Memb. Sci. 525 (2017) 107–115.
542 doi:10.1016/j.memsci.2016.10.035.
543 [26] M. Micari, A. Cipollina, F. Giacalone, G. Kosmadakis, M. Papapetrou, G. Zaragoza, G. Micale, A.
544 Tamburini, Towards the first proof of the concept of a Reverse ElectroDialysis - Membrane Distillation
545 Heat Engine, Desalination. 453 (2019) 77–88. doi:10.1016/j.desal.2018.11.022.
546 [27] D.H. Kim, B.H. Park, K. Kwon, L. Li, D. Kim, Modeling of power generation with thermolytic reverse
547 electrodialysis for low-grade waste heat recovery, Appl. Energy. 189 (2017) 201–210.
548 doi:10.1016/j.apenergy.2016.10.060.
549 [28] M. Bevacqua, A. Tamburini, M. Papapetrou, A. Cipollina, G. Micale, A. Piacentino, Reverse
550 electrodialysis with NH4HCO3-water systems for heat-to-power conversion, Energy. 137 (2017)
551 1293–1307. doi:10.1016/j.energy.2017.07.012.
552 [29] P. Palenzuela, M. Micari, B. Ortega-Delgado, F. Giacalone, G. Zaragoza, D.-C. Alarcón-Padilla, A.
553 Cipollina, A. Tamburini, G. Micale, Performance Analysis of a RED-MED Salinity Gradient Heat
554 Engine, Energies. 11 (2018) 3385. doi:10.3390/en11123385.
555 [30] B. Ortega-Delgado, F. Giacalone, P. Catrini, A. Cipollina, A. Piacentino, A. Tamburini, G. Micale,
556 Reverse electrodialysis heat engine with multi-effect distillation: Exergy analysis and perspectives,
557 Energy Convers. Manag. 194 (2019) 140–159. doi:10.1016/j.enconman.2019.04.056.
558 [31] M. Shahid, X. Xue, C. Fan, B.W. Ninham, R.M. Pashley, Study of a Novel Method for the Thermolysis
559 of Solutes in Aqueous Solution Using a Low Temperature Bubble Column Evaporator, J. Phys. Chem.
560 B. 119 (2015) 8072–8079. doi:10.1021/acs.jpcb.5b02808.
561 [32] F. Giacalone, F. Vassallo, L. Griffin, M.C. Ferrari, G. Micale, F. Scargiali, A. Tamburini, A. Cipollina,
562 Thermolytic reverse electrodialysis heat engine: model development, integration and performance
563 analysis, Energy Convers. Manag. (2019). doi:10.1016/j.enconman.2019.03.045.
564 [33] A. Cipollina, G. Micale, A. Tamburini, M. Tedesco, L. Gurreri, J. Veerman, S. Grasman, 5 – Reverse
565 electrodialysis: Applications, in: Sustain. Energy from Salin. Gradients, 2016: pp. 135–180.
566 doi:10.1016/B978-0-08-100312-1.00005-5.

567 [34] Z. Meng, J.H. Seinfeld, P. Saxena, Y.P. Kim, Atmospheric Gas-Aerosol Equilibrium: IV.
568 Thermodynamics of Carbonates, Aerosol Sci. Technol. 23 (1995) 131–154.
569 doi:10.1080/02786829508965300.
570 [35] F. Giacalone, P. Catrini, A. Tamburini, A. Cipollina, A. Piacentino, G. Micale, Exergy analysis of
571 reverse electrodialysis, Energy Convers. Manag. 164 (2018) 588–602.
572 doi:10.1016/j.enconman.2018.03.014.
573 [36] M.L. La Cerva, M. Di Liberto, L. Gurreri, A. Tamburini, A. Cipollina, G. Micale, M. Ciofalo, Coupling
574 CFD with a one-dimensional model to predict the performance of reverse electrodialysis stacks, J.
575 Memb. Sci. 541 (2017) 595–610. doi:10.1016/j.memsci.2017.07.030.
576